FOCUS ISSUE

3D PRINTING OF BIOMEDICAL MATERIALS AND DEVICES

Hydrogel-integrated 3D-printed poly(lactic acid) scaffolds for bone tissue engineering

Mitun Das[1,2,4], Orna Sharabani-Yosef[3], Noam Eliaz[1,a)], Daniel Mandler[2,a)]

[1] Department of Materials Science and Engineering, Tel-Aviv University, 6997801 Tel Aviv, Israel
[2] Institute of Chemistry, The Hebrew University of Jerusalem, 9190401 Jerusalem, Israel
[3] Department of Biomedical Engineering, Tel-Aviv University, 6997801 Tel Aviv, Israel
[4] CSIR – Central Glass and Ceramic Research Institute, Kolkata 700032, India
[a)] Address all correspondence to these authors. e-mails: neliaz@tau.ac.il; daniel.mandler@mail.huji.ac.il

There is currently a high demand for synthetic biodegradable scaffolds with enhanced osteogenic and angiogenic performance for the regeneration of large-size bone defects. Here, hybrid scaffolds were prepared by integrating either alginate or alginate–bioglass composite hydrogels with a 3D-printed poly(lactic acid) (PLA) porous structure. The as-deposited PLA scaffolds were surface treated with polyacrylic acid (PAA), which significantly enhanced the PLA scaffold's wettability. The surface-modified PLA scaffolds integrated well with hydrogels and provided shape and mechanical rigidity to the hydrogel. In phosphate-buffered saline, the lowest weight loss during 21-days immersion was measured for the PLA scaffold, while alginate–bioglass scaffolds lost ~ 1.9% weight during the first 7 days of immersion. In vitro cytocompatibility tests indicated good cell viability and cell proliferation on the scaffolds. The bioglass-containing hybrid scaffold promoted osteogenic differentiation and calcium mineralization. The excellent biocompatibility, good mechanical stability of the hydrogel, and shape retention of the novel hybrid scaffolds with cell-laden alginate could make them attractive for large bone regeneration.

Introduction

Excessive bone damage due to trauma and injury and repair of congenital defects or bone loss following resection of tumors require external intervention in the form of a scaffold for regeneration and restoration of bone function [1, 2]. Bone grafting is one of the most common procedures. The global market for bone graft substitutes is expected to grow at a compound annual rate of 6.25% and will exceed 5 billion US dollars by 2027 [3]. Among different transplant procedures, autogenic (i.e., taken from the intended host's own body) bone graft remains the gold standard. However, this concept suffers from some significant drawbacks, such as the need for two-stage operation, relatively high cost, donor site morbidity, and limited availability [4, 5]. Hence, in many cases, an autograft is not suitable for the treatment of large-size bone defects. To meet the demand, tremendous attention has been given to bone tissue engineering (BTE), where porous synthetic biomaterials (scaffolds) are seeded with cells and/or bioactive molecules to promote both osteogenic and

angiogenic performance [1, 2, 6–8]. Ideally, a scaffold for BTE should be biocompatible, porous, biodegradable (to be replaced over time by the host tissue), osteoconductive, osteoinductive, and carry the mechanical load to act as an extracellular matrix [8, 9]. Besides chemistry, scaffold architecture, including pore size, shape, volume, and interconnectivity, is essential for the scaffold's in vivo performance [10, 11]. Among different processing techniques, additive manufacturing (AM) has become increasingly popular due to its capability to form scaffolds of complex architectures directly from a computer-aided design (CAD) file [7, 8, 12–14]. Scaffolds prepared by AM based on computer tomography (CT) or magnetic resonance imaging (MRI) of the defect site can match more appropriately [15].

In recent years, synthetic scaffolds made of biodegradable polymers have received considerable attention for BTE [16]. The 3D-printed synthetic polymer scaffolds with interconnected porous architecture have been preferred because of their appropriate mechanical properties, controlled degradation

with non-toxic hydrolysis products, biocompatibility, and no adverse immune response [17]. Among the synthetic polymers, poly(lactic acid) (PLA) has been used extensively for biomedical applications because of its excellent mechanical properties, ease of fabrication, good biocompatibility, and biodegradability [18]. Furthermore, PLA can easily be processed into scaffolds using fuse deposition modeling (FDM)-based AM [19, 20]. The US Food and Drug Administration (FDA) has approved PLA-based medical devices for orthopedic and dental applications in the form of screws, pins, washers, darts, sutures, etc. [18, 21]. However, PLA's main drawbacks as a scaffold material for BTE are its low hydrophilicity and lack of active functional groups for cell growth and proliferation [18, 22]. To improve bioactivity, researchers have modified the surface of 3D porous PLA scaffolds using chemical treatment for entrapment of biomacromolecules, coating by bioactive ceramics or mussel-inspired material, and cold plasma-based techniques [23–31].

In recent years, hydrogel-based scaffolds have gained interest for BTE [32, 33]. Alginate is one such natural polymer studied in detail for bone tissue regeneration in the form of injectable or composite hydrogels [34, 35]. Alginate is a linear polysaccharide soluble in water, forms viscoelastic gels under specific conditions, and interacts easily with proteins, hydrophilic, cytocompatible, and non-immunogenic [34–36]. Thus, alginate hydrogel has found applications in drug carrying [37], wound healing [38], tissue engineering [39], and minimum invasive treatment for bone regeneration [40, 41]. However, hydrogel's inherent low mechanical strength hinders its use as a scaffold for large bone defects. Several strategies like double-network, topological, nanocomposites, macromolecular microsphere composite, and supramolecular hydrogels have been developed to enhance the mechanical properties of hydrogel-based scaffolds [42–44]. Studies have shown that the incorporation of inorganic particles such as calcium phosphates [45], bioglass, calcium carbonate, and silica nanoparticles (NPs) enhance the mechanical properties and mineralization of hydrogels [33, 35]. Yet, adequate mechanical strength for structural support and osseointegration of hydrogel scaffolds for bones is still a challenge for clinical use.

Some reports have shown an alginate coating on AM'ed polycaprolactone (PCL), where alginate hydrogel was used to encapsulate cells and/or to carry growth factors [41, 46]. Kundu et al. [46] have shown AM'ed PCL and chondrocyte cell-encapsulated alginate hydrogel-based bio-hybrid scaffold for cartiladge tissue engineering. They have used a 3D printer with multihead deposition system (MHDS) where a porous PCL layer was deposited, and simultaneously cell-laden alginate was dispensed in spaces between lines of the PCL layer. The objective of such construct was to provide mechanical stability to the cell-laiden hydrogel for a longer period of time. Some reports are also available on alginate coating on AM'ed

PLA scaffolds where the main objective was to improve the bioactivity of PLA [47, 48]. In a recent report, Fernández-Cervantes et al. [48] fabricated sodium alginate/hydroxyapatite coating on 3D-printed PLA scaffold designed based on a bone remodeling mold. Mineralization in simulated body fluid (SBF) of such composite scaffolds showed an improvement in compressive strength.

Here, we use a novel hybrid strategy for scaffold fabrication where the 3D-printed porous PLA structure provides rigidity to the hydrogel and fits properly at defect sites, while the cell-laden alginate/alginate–bioglass creates an environment for osteoblast cells to proliferate. Furthermore, the surface of the PLA scaffold was modified with polyacrylic acid (PAA) [23] to improve the hydrophilicity of the PLA surface and ensure complete penetration and integration of the viscous hydrogel into the porous PLA structure. The grafted PAA on the PLA surface would likely form chemical bonding with alginate [49]. The incorporation of bioglass is expected to improve both the stability of alginate and bioactivity. The in vitro cell–material interactions were studied for cytotoxicity, cell morphology, and osteogenic differentiation. The hybrid composite scaffold containing bioglass was found to promote human fetal osteoblast cells (hFOB) proliferation and differentiation into bone-forming cells.

Results and discussion

Phase analysis

XRD analysis was carried out to analyze the phases present in the specimens. Figure 1 shows the XRD patterns of bioglass powder (BG), 3D-printed PLA (PLA), PAA-treated PLA (PLA-S), alginate-coated PLA (PLA-Alg), and alginate–bioglass-coated PLA (PLA-Alg-BG) specimens. XRD analysis of the sol–gel-derived bioactive glass (45S5) (Fig. 1a) revealed $Na_2CaSi_2O_6$ (Combeite) (file #012-8759) as a major phase, with some minor reflections of crystalline apatite-like phosphorus-rich phase $NaCa_3(PO_4)SiO_4$ (file #006-2364). No major unreacted phases in the BG powder could be detected, as previously reported [50, 51]. The diffraction pattern of 3D-printed PLA sample (Fig. 1b) showed a broad hump, indicating the material's semi-crystalline/amorphous nature. Surprisingly, PLA surface treated with PAA (Fig. 1c) showed distinct crystalline peaks at $2\theta = 14.7, 16.6, 19.1$, and $22.3°$, coinciding with α-poly(ʟ-lactide), as reported by Sasaki et al. [52]. These results indicate that PAA grafted on the PLA surface was transformed from an amorphous layer into a crystalline α-poly(ʟ-lactide). Furthermore, the alginate-coated and alginate–bioglass-coated samples (Fig. 1d, e) showed no peaks related to alginate, indicating that the alginate hydrogel was amorphous in nature. However, crystalline α-poly(ʟ-lactide) peaks can be seen in both hydrogel-coated specimens. Distinct

Figure 1: XRD patterns of: (a) sol–gel-derived bioglass (45S5) powder, (b) 3D-printed PLA, (c) PAA-treated PLA, (d) alginate-coated PLA, (e) alginate–bioglass-coated PLA.
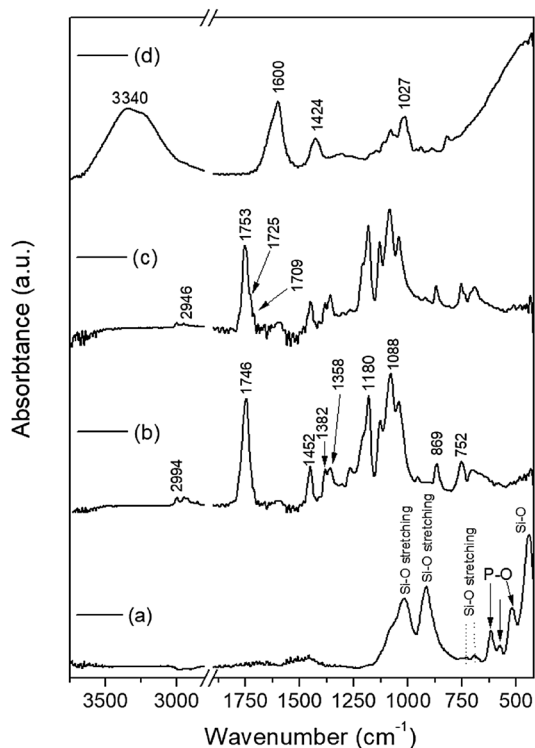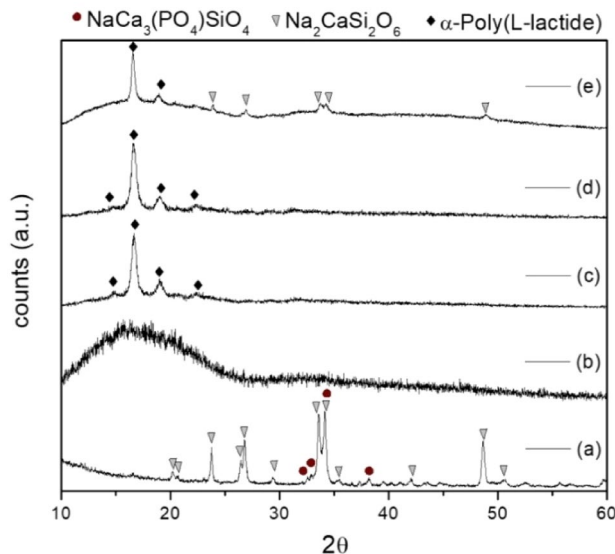

Figure 2: FTIR spectra of: (a) sol–gel-derived bioglass (45S5) powder, (b) 3D-printed PLA, (c) PAA-treated PLA, (d) alginate-coated PLA.

peaks of bioglass are noticed in the alginate–bioglass-coated sample.

FTIR was also conducted to analyze the bioglass and polymers. Figure 2 shows the IR absorption spectrum of bioglass, PLA, PAA-treated PLA, and alginate-coated PLA samples. The FTIR spectrum of the sol–gel-synthesized BG powder showed two broad peaks at 1017 and 915 cm^{-1}, associated with Si–O–Si asymmetric stretching vibration and Si–O-non-bridging oxygen band (NBO), respectively [50]. The large peak of NBO indicates Combeite's presence in the structure since Combeite contains more NBO bonding compared to amorphous 45S5 [50]. The small doublets at 693 and 730 cm^{-1} are assigned to the symmetric Si–O–Si stretching vibration in the crystalline silicate. The strong peak at 450 cm^{-1} is attributed to the Si–O vibration modes in the SiO_4 group, which suggests amorphous silicate presence [53]. The peaks at 520, 578, and 615 cm^{-1} are assigned to bending P–O bond [50]. In the PLA sample (Fig. 2b), the peaks around 3000–2800 cm^{-1} are attributed to the stretching vibrations of the CH_3 group. The intense peak at 1746 cm^{-1} corresponds to the C=O stretching vibration of the ester group. The band at 1452 cm^{-1} is assigned to the CH_3 bending, and the C–H deformation vibration peaks are observed at 1382 (δ_{as} CH_3) and 1358 cm^{-1} (δ_s CH_3) [54]. The symmetric and asymmetric stretching vibrations of C–O–C are evident, respectively, at 1180 and 1088 cm^{-1} [55]. The amorphous and crystalline phases of PLA are noted at 871 and 756 cm^{-1}, respectively [54]. The IR bands for the PAA-coated PLA sample (Fig. 2c) showed peaks similar to PLA. However, small shoulders at 1709 and 1725 cm^{-1} are assigned to the C=O stretching mode of the PAA carbonyl group [56]. The FTIR spectrum of alginate-coated PLA is shown in Fig. 2d. The spectrum clearly shows the characteristic peaks of alginate. The peaks at 3340, 1600, 1424, and 1027 cm^{-1} are attributed to –OH stretching, –COOH (asymmetric stretching), –COOH (symmetric stretching), and C–O–C (asymmetric stretching), respectively [57].
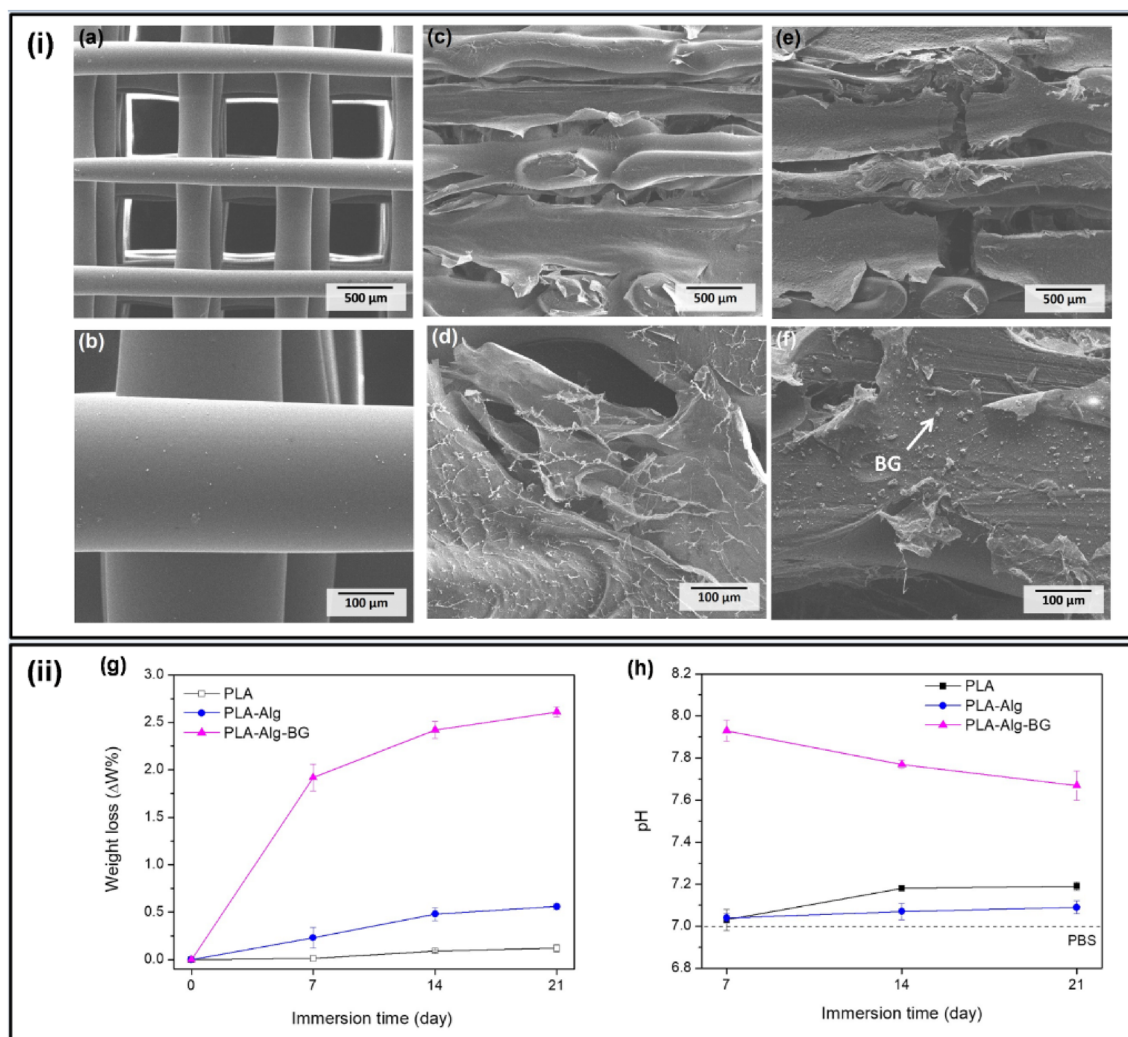
Figure 3: (i) Typical SEM images of 3D-printed PLA (a, b), alginate coating on PLA (c, d), and alginate–bioglass coating on PLA (e, f); (ii) Degradation behavior of scaffolds in PBS up to 21 days of immersion: (g) change in weight loss with immersion time, (h) change in pH over time. Samples in triplicate (*n* = 3) were used for each data point. Related SEM images of the scaffolds after 21 days of immersion in PBS are shown in Fig. S1.

Morphological characterization

Typical SEM micrographs of 3D-printed PLA, PLA-Alg, and PLA-Alg-BG scaffolds are shown in Fig. 3. The micrographs of as-printed PLA scaffolds show smooth surfaces with fully interconnected porosity (Fig. 3a, b). The average strut thickness and pore size of the 3D-printed PLA scaffolds were measured from SEM images as 301 ± 16 μm and 685 ± 78 μm, respectively. The total porosity of these scaffolds was ~44%. The hybrid scaffold prepared by integrating 3D-printed PLA with alginate hydrogel is shown in

Fig. 3c, d. The morphology clearly shows that hydrogel was able to penetrate entirely inside of the porous structure. Similarly, the morphology of the PLA-Alg-BG scaffold is shown in Fig. 3e, f. For the SEM study, the hydrogel-integrated samples were lyophilized. The porous nature of the hydrogel structure can be seen in all the hybrid scaffolds. The bioglass-incorporated hydrogel clearly shows homogeneously distributed bioglass particles in the hydrogel matrix.

TABLE 1: Contact angle data and calculated surface energy of 3D-printed PLA before and after surface modification with PAA. γ_S^d and γ_S^p are the dispersive and polar components of the surface energy of the solid, respectively.

Sample	DI water	Ethylene glycol	γ_S^d (mN/m)	γ_S^p (mN/m)	Total surface energy (mN/m)
PLA	$76.1° \pm 4.5°$	$48.2° \pm 1.8°$	24.8 ± 0.0	9.4 ± 0.0	34.2 ± 0.0
PLA-PAA	$61.9° \pm 2.8°$	$43.8° \pm 2.9°$	9.3 ± 0.0	30.3 ± 0.0	39.6 ± 0.0

Surface energy and degradation behavior

The contact angles of DI water and ethylene glycol on PLA and PLA-PAA samples are reported in Table 1 along with the total surface energy. The contact angle of DI water was reduced significantly from 76 to 62° after surface treatment with PAA. The total surface energy of PLA increased from 34 to 40 mN/m in PLA-PAA. Thus, PAA treatment enhanced PLA's wettability and resulted in hydrogel penetration into the porous scaffold. The calculated average porosity of the 3D-printed PLA scaffolds was 56±4%.

The interconnected porous PLA structures by FDM printing is an appealing approach due to its low cost, ease of processing, and accuracy. Due to the low wettability of the as-deposited porous PLA scaffolds, alginate, and alginate–bioglass hydrogels penetration were not easy. The PAA surface treatment of PLA scaffolds eliminated this shortfall. The hydrogel-integrated PLA scaffolds were immersed into Dulbecco's PBS. The subsequent weight losses and pH variation of the immersion solutions were measured for up to 21 days. The results presented in Fig. 3g clearly show that the change in weight loss in as-deposited PLA scaffolds was significantly low compared with the hydrogel-integrated scaffolds. The maximum weight loss was observed in PLA-Alg-BG scaffolds. The ionic dissolution of bioglass particles in PBS seems to be a significant contributor to the initial 7 days' sharp weight loss. The 45S5 bioglass contains non-bridging oxygen atoms, which result in an open silicate network, leading to easy penetration of water-based solutions and the subsequent dissolution of glass and release of ions [58]. The release of cations (Ca^{2+}, Na^+) from the glass surface consequently increased the solution's pH. It is worth noting that the rate of weight changes from 7 to 21 days of immersion was nearly similar for both PLA-Alg and PLA-Alg-BG hydrogel scaffolds. Figure 3h shows the pH variation in PBS solutions containing PLA, PLA-Alg, and PLA-Alg-BG scaffolds as a function of time. A slight increase in pH was observed in the immersion solutions containing PLA and PLA-Alg scaffolds. In the case of PLA-Alg, the immersion solution's pH was nearly constant, whereas the pH of the PLA-containing solution increased from 7.03 to 7.18 after 21 days of immersion. However, the PBS containing PLA-Alg-BG scaffold showed pH of 7.93 after 7 days of immersion, which gradually decreased to pH 7.67 after 21 days of immersion. The sharp increase in the immersion solution's pH after 7 days is due to the rapid release of ions from the bioglass into the solution. The weight-loss behavior during 7 days also confirms the rapid dissolution of bioglass from the PLA-Alg-BG scaffold. However, with increasing immersion time, the cleavage of Si–O–Si bonds led to hydrated silica (SiOH)-rich gel layer on the bioglass particles, and the subsequent ion exchange helped forming CaP-rich layer [51]. Thus, the formation of a barrier layer and deposition of Ca and P ions from solution resulted in a slight decrease of the pH in the immersion solution.

In vitro cell viability, proliferation and osteogenic differentiation

The in vitro cytotoxicity of PLA, PLA-Alg, and PLA-Alg-BG scaffolds and the effect of those materials on cells proliferation and osteogenic differentiation were evaluated using an indirect MTT assay. Of similar dimensions, all scaffolds were immersed in a GM for 48 h at 37 °C, which allows partial leaching from the degradable scaffolds. The extracted media from individual scaffolds were used to study cytotoxicity and proliferation of hFOB cells. As a control, hFOB cells were cultured in fresh GM. Figure 4a shows the viability and proliferation of hFOB cells after 3, 5, and 7 days. It is clear that none of the media extracted from the scaffolds were cytotoxic and that in all the cases, cells were proliferated throughout the whole culture duration. In the MTT assay, the measured optical density of the solution is proportional to the number of viable cells. Initially, the maximum cell viability was observed in the PLA extracted medium; cell proliferation was significantly higher ($p < 0.05$) than for the other materials during initial 3 days of culture. Cell proliferation in media extracted from PLA and PLA-Alg-BG scaffolds was comparatively similar over time. The maximum cell proliferation was observed in PLA-Alg-BG scaffolds after 7 days of culture. It is also evident that all samples were cytocompatible; cells proliferated throughout culture duration in all the media extracted from different scaffolds. Fluorescence micrographs of cells cultured for 5 days using the media extracted from the scaffolds are shown in Fig. 4b. The hFOB cells were stained with Phalloidin and DAPI, emitting green and blue fluorescence, respectively. The Phalloidin binds to the actin filaments in the cytoplasm, while DAPI stains the cell nuclei. In all cases, cells were flattened and connected with lamellipodia and filopodia, indicating cell viability.

Osteoblast differentiation is one of the key steps in bone regeneration. The effect of scaffold composition on the in vitro differentiation of hFOB cells into extracellular matrix mineralization was qualitatively studied by Alizarin red-staining assay. In the Alizarin red assay, the calcified bone nodules in the cells become stained in red. In this study, hFOB cells were directly seeded on the scaffolds and cultured for up to 14 days. Besides, a set of scaffolds without cells were cultured and stained by Alizarin red to normalize the assay results. Figure 4c shows Alizarin stain assay results, clearly suggesting that cells were differentiated significantly on the PLA-Alg-BG scaffold compared to the other two scaffolds. The ions released from bioglass particles should influence the osteogenic differentiation.

In this context, Kundu et al. [46] recently studied a hybrid composite scaffold where a 3D-printed porous PCL layer was filled with cartilaginous cell-laden alginate, showing reduced cell viability during multipayer stacking of the PCL layer. The reduced cell viability was claimed to be due to high temperature
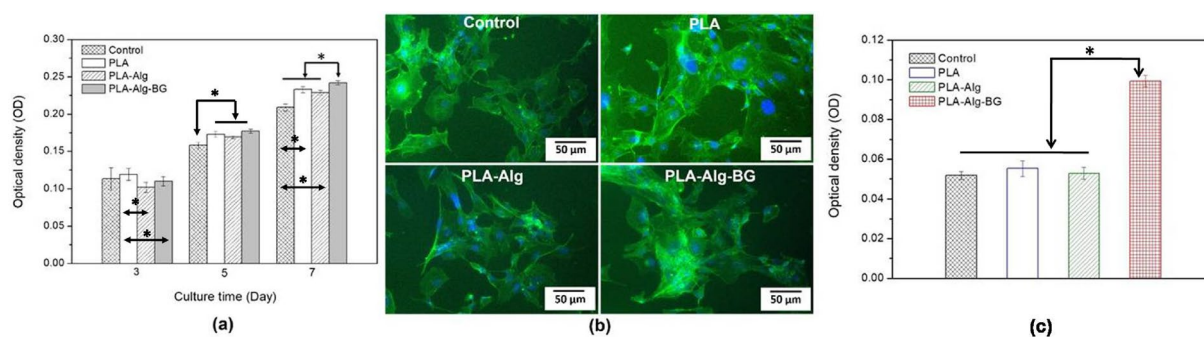
Figure 4: Osteoblast cells cultured in media extracted from PLA, PLA-Alg, PLA-Alg-BG scaffolds and fresh media for control. (a) Cell viability and proliferation of cells expressed by MTT assay for different culture periods (*$p < 0.05$, indicating statistical significance). (b) Fluorescence micrographs of hFOB cells cultured for 5 days, stained with DAPI (blue) and Phalloidin (green). (c) Osteogenic differentiation evaluated by qualitative analysis of Alizarin red staining of calcium (*$p < 0.05$).

produced during deposition of PCL layer. In our present approach, we constructed the 3D-printed PLA framework, followed by surface treatment, to ensure complete penetration of alginate hydrogel carrying bioglass or cells. We have demonstrated the cytocompatibility and excellent osteogenic potential of a hybrid scaffold consisted of 3D-printed PLA porous skeleton structure and alginate–bioglass hydrogel, which could become a prospective system for bone tissue regeneration.

Conclusions

In this study, we demonstrated a novel hydrogel-integrated PLA-based hybrid scaffold. The PLA would provide mechanical stability and retain the shape of the hydrogel, which is essential for large-size bone defects. On the other hand, the hydrogel can be used as a cell-laden matrix to provide a microenvironment for carrying cells, drugs, growth factors, or inorganic cues. The interconnected porous PLA scaffolds, generated using an inexpensive 3D printer, were integrated well with alginate hydrogel after surface treatment with PAA. Surface treatment significantly enhanced hydrophilicity of PLA that helps the alginate and alginate–bioglass solution to penetrate into the porous PLA structure. Initially, the PLA–alginate–bioglass scaffolds degraded rapidly compared to other scaffolds because of the rapid dissolution of bioglass. In vitro results indicated that the bioglass–alginate composite supports cell proliferation. The presence of bioglass in the system significantly promotes osteogenic differentiation of preosteoblasts. Overall, the concept of a hybrid composite scaffold with cell-laden hydrogel holds promise for bone regeneration for large bone defects.

Materials and methods

3D-printed PLA scaffolds and 45S5 bioglass

The interconnected porous PLA scaffolds with dimensions of $9.4 \times 9.4 \times 5.2 \text{ mm}^3$ were manufactured in an FDM-based 3D

printer (MakerBot Replicator, USA). The initial design of the scaffold with 0/90 lay down pattern, strut diameter of 400 μm, and a distance of 600 μm between two struts, was prepared using SolidWorks® 3D CAD software (Fig. 5). The 45S5 bioglass (BG), with a composition of 45 wt% SiO_2, 24.5 wt% Na_2O, 24.5 wt% CaO and 6 wt% P_2O_5, was prepared via a sol–gel route, as described elsewhere [50]. In brief, an aqueous solution of tetraethyl orthosilicate (TEOS, $Si(OC_4H_9)_4$, Sigma Aldrich), triethylphosphite ($P(OEt)_3$, $P(C_2H_5O)_3$, Sigma Aldrich), calcium nitrate tetrahydrate ($Ca(NO_3)_2 \cdot 4H_2O$, Sigma Aldrich), and sodium nitrate ($NaNO_3$, Sigma Aldrich) was prepared by adding these materials consecutively at time intervals of 30 min under continuous magnetic stirring at room temperature. HNO_3 (0.1 M) was used to hydrolyze TEOS and $P(OEt)_3$. The resultant sol was kept at room temperature for about 10 days, aged at 70 °C for 72 h, and finally dried in oven at 120 °C for 24 h, allowing the removal of gaseous byproducts. The dried gel was thermally treated in air at 800 °C for 12 h. The thermally treated powder was ground and passed through sieves; the end particle size was below 5 μm.

Surface treatment of the PLA scaffold and hydrogel coating

The 3D-printed PLA scaffolds were placed in a UV-Ozone cleaning chamber (UVOCleaner®, CA, USA) for 5 min in order to activate the surface. Grafting of PAA on PLA was performed by dipping the porous scaffold into a solvent/non-solvent miscible mixture of chloroform/ethanol (1/9 v/v) for 2 min followed by immersion of the scaffold in a 0.1 wt% solution of PAA in water for 2 h [24]. The samples were then soaked in water for 30 min to remove any extra PAA and then dried under a vacuum for 12 h.

The surface-treated PLA scaffolds were further coated with either 2% (w/v) alginate or alginate–bioglass. Bioglass at a concentration of 5 g/L was used for an alginate–bioglass suspension. The PAA-coated PLA scaffolds were dip coated in either alginate
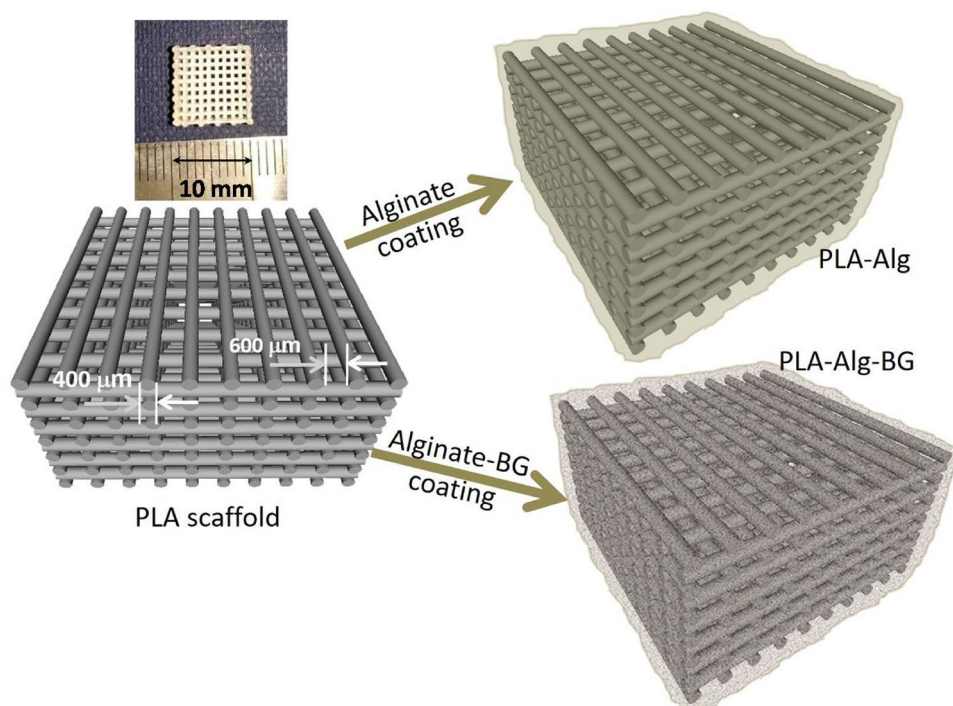
Figure 5: CAD design of the scaffold and schematics of the hydrogel-incorporated scaffolds. CCD image: The actual 3D-printed scaffold.

or alginate–bioglass suspension for 5 min, followed by immersion in 0.1 M CaCl$_2$ (Sigma Aldrich) solution for 1 h. Figure 5 shows schematics of alginate-incorporated PLA (PLA-Alg) and alginate–bioglass-incorporated PLA (PLA-Alg-BG) scaffolds.

Material characterization

The structures of the 3D-printed PLA, alginate and alginate–bioglass-coated specimens were analyzed by X-ray diffraction (XRD) and Fourier transform infrared (ATR-FTIR) spectroscopy (Nicolet iS10, Thermo Scientific). The surface energy of both as-printed PLA and PAA-grafted PLA specimens was determined by measuring the contact angles of two different liquids—DI water and ethylene glycol—using a drop shape analyzer (DSA25E, KRÜSS GmbH) [59].

Degradation in phosphate-buffered saline

The degradation behavior of 3D-printed PLA, PLA-Alg, and PLA-Alg-BG scaffolds was evaluated in 1X phosphate-buffered saline (PBS). All scaffolds were initially lyophilized to determine the initial weight (W_0) and were subsequently immersed in 10 mL of PBS for 7, 14, and 21 days. The vials containing samples and PBS were kept on a flat plate orbital shaker (QSD OS20, Lumitron, Israel), moving at a speed of 100 rpm. After soaking

for different durations, the samples were removed from the buffer solution, gently washed with DI water, and lyophilized. The degradation of the scaffolds was measured from the percentage weight change ($\Delta W\%$) by monitoring the weight before (W_0) and after (W_f) immersion using a high-precision balance (ES225SM-DR, Precisa) with 10 μg sensitivity. The percentage weight change was calculated using Eq. 1:

$$\Delta W\% = \left(\frac{W_0 - W_f}{W_0} \right) \times 100. \qquad (1)$$

The variation of pH in the buffer solution due to degradation of scaffolds was also monitored using a pH meter. Samples in triplicate ($n = 3$) were used for the degradation study.

In vitro cell culture study

The cytotoxicity and cell proliferation on 3D-printed PLA and hydrogel-coated PLA were assessed using hFOBcell line (ATCC,USA). Prior to the cell culture experiment, the porous PLA samples were sterilized in 70% ethanol and UV radiation for 30 min. The CaCl$_2$ solution, alginate, and alginate–bioglass suspensions were prepared under sterile conditions prior to preparation of the hydrogel-coated samples. Before PLA-Alg-BG scaffold preparation, the bioglass powder was preconditioned by immersing in cell culture medium (without serum) for 48 h [58].

The hFOB cells were cultured in growth media (GM) containing 90% 1:1 Dulbecco's Modified Eagle Medium:Ham's F-12 (DMEM/F12, Biological Industries) with 2.5 mM L-Glutamine (Biological Industries), 0.3 mg/mL G418 (Apollo Scientific), and 10% Fetal Bovine Serum (FBS) (Biological Industries). Cells were cultured in an incubator at 37 °C and 5% CO_2. The cytotoxicity and cell proliferation behavior were studied using a non-contact method. Sterile scaffolds of similar sizes were immersed in the GM at 37 °C for 48 h and used the supernatant liquids from all specimens for cell culture. The fresh GM was considered as control with respect to supernatant liquids collected from the specimens.

The viability and proliferation of hFOB cells were quantitatively assessed using 3-(4,5-dimethylthiazol-2-yl)-2,5-diphenyl tetrazolium bromide (MTT, Apollo Scientific, UK). Furthermore, the cell morphologies in 24-well plate were studied by staining the cells with Phalloidin (Phalloidin-iFluor 488, Abcam,USA) and DAPI (Abcam,USA) as per the company protocol. The cells in the well plate were detected using a fluorescent microscope (Axiovert 40CFL, Zeiss) at excitation/emission of 493/517 nm and 358/461 nm for Phalloidin and DAPI, respectively.

For Alizarin red staining assay, hFOB cells were directly seeded on the scaffolds and were cultured in GM. After 14 days of culture, cells were washed with PBS thrice, followed by fixation with 4% formaldehyde for 15 min and were then rinsed three times with DI water. The scaffolds were then immersed in 40 mM Alizarin red S (Apollo Scientific, UK) solution (pH 4.2) for 10 min. After that, scaffolds were washed several times with DI water to remove unbound dyes. To quantify the calcification, the dye attached with calcified bone nodules was dissolved with 10% (w/v) acetic acid solution. The optical density of the extracted solution was measured using a spectrophotometer at 405 nm wavelength. Each type of scaffold was tested in triplicate ($n = 3$).

Statistical analysis was carried out using Student's t test pairwise, with $p < 0.05$ being considered statistically significant.

Acknowledgments

Data availability

The raw/processed data required to reproduce these findings cannot be shared at this time as the data also form part of an ongoing study.

Declarations

Conflict of interest The authors declare no conflict of interest.

Supplementary Information

The online version supplementary material available at https://doi.org/10.1557/s43578-021-00201-w.

References

1. W. Wang, K.W.K. Yeung, Bioactive materials bone grafts and biomaterials substitutes for bone defect repair: A review. Bioactive Mater. **2**, 224–247 (2017)

2. Ž.P. Kačarević, P. Rider, S. Alkildani, S. Retnasingh, M. Pejakić, R. Schnettler, M. Gosau, R. Smeets, O. Jung, M. Barbeck, An introduction to bone tissue engineering. Int. J. Artif. Organs **43**, 69–86 (2020)

3. Bone graft substitute market research report – Global forecast till 2027, Market Research Future®, July 2019. https://www.marketresearchfuture.com/reports/bone-graft-substitutes-market-1195 accessed 23 Feb 2020.

4. V. Campana, G. Milano, E. Pagano, M. Barba, C. Cicione, G. Salonna, W. Lattanzi, G. Logroscino, Bone substitutes in orthopaedic surgery: from basic science to clinical practice. J. Mater. Sci. Mater. Med. **25**, 2445–2461 (2014)

5. G. Fernandez de Grado, L. Keller, Y. Idoux-Gillet, Q. Wagner, A.M. Musset, N. Benkirane-Jessel, F. Bornert, D. Offner, Bone substitutes: A review of their characteristics, clinical use, and perspectives for large bone defects management. J. Tissue Eng. **9**, 1–18 (2018)

6. J. Henkel, M.A. Woodruff, D.R. Epari, R. Steck, V. Glatt, I.C. Dickinson, P.F.M. Choong, M.A. Schuetz, D.W. Hutmacher, Bone regeneration based on tissue engineering conceptions— A 21st century perspective. Bone Res. **1**, 216–248 (2013)

7. A. Wubneh, E.K. Tsekoura, C. Ayranci, H. Uludağ, Current state of fabrication technologies and materials for bone tissue engineering. Acta Biomater. **80**, 1–30 (2018)

8. S. Bose, S. Vahabzadeh, A. Bandyopadhyay, Bone tissue engineering using 3D printing. Mater. Today **16**, 496–504 (2013)

9. A. Grémare, V. Guduric, R. Bareille, V. Heroguez, S. Latour, N. Lheureux, J.-C. Fricain, S. Catros, D. Le Nihouannen, Characterization of printed PLA scaffolds for bone tissue engineering. J. Biomed. Mater. Res. A **106**, 887–894 (2018)

10. S. Gómez, M.D. Vlad, J. López, E. Fernández, Design and properties of 3D scaffolds for bone tissue engineering. Acta Biomater. **42**, 341–350 (2016)

11. A. Entezari, I. Roohani, G. Li, C.R. Dunstan, P. Rognon, Q. Li, X. Jiang, H. Zreiqat, Architectural design of 3D printed scaffolds controls the volume and functionality of newly formed bone. Adv. Healthcare Mater. **8**, 1801353 (2019)

12. R. Fairag, D.H. Rosenzweig, J.L. Ramirez-Garcialuna, M.H. Weber, L. Haglund, Three-dimensional printed polylacticacid scaffolds promote bone-like matrix deposition in vitro. ACS Appl. Mater. Interfaces **11**, 15306–15315 (2019)

13. S.-B. Hong, N. Eliaz, E.M. Sachs, S.M. Allen, R.M. Latanision, Corrosion behavior of advanced Ti-based alloys made by three-dimensional printing (3DP™) for biomedical applications. Corros. Sci. **43**, 1781–1791 (2001)

14. S.-B. Hong, N. Eliaz, G.G. Leisk, E.M. Sachs, R.M. Latanision, S.M. Allen, A new Ti-5Ag alloy for customized prostheses by three-dimensional printing (3DP™). J. Dent. Res. **80**, 860–863 (2001)

15. M. Das, V.K. Balla, T.S.S. Kumar, I. Manna, Fabrication of biomedical implants using laser engineered net shaping (LENS™). Trans. Indian Ceram. Soc. **72**, 169–174 (2013)

16. S. Stratton, N.B. Shelke, K. Hoshino, S. Rudraiah, S.G. Kumbar, Bioactive polymeric scaffolds for tissue engineering. Bioactive Mater. **1**, 93–108 (2016)

17. G. Ratheesh, J.R. Venugopal, A. Chinappan, H. Ezhilarasu, A. Sadiq, S. Ramakrishna, 3D fabrication of polymeric scaffolds for regenerative therapy. ACS Biomater. Sci. Eng. **3**, 1175–1194 (2017)

18. G. Narayanan, V.N. Vernekar, E.L. Kuyinu, C.T. Laurencin, Poly (lactic acid)-based biomaterials for orthopaedic regenerative engineering. Adv. Drug Deliv. Rev. **107**, 247–276 (2016)

19. A. Gregor, E. Filová, M. Novák, J. Kronek, H. Chlup, M. Buzgo, V. Blahnová, V. Lukášová, M. Bartoš, A. Nečas, J. Hošek, Designing of PLA scaffolds for bone tissue replacement fabricated by ordinary commercial 3D printer. J. Biol. Eng. **11**, 31 (2017)

20. S.R. Rajpurohit, H.K. Dave, Analysis of tensile strength of a fused filament fabricated PLA part using an open-source 3D printer. Int. J. Adv. Manuf. Technol. **101**, 1525–1536 (2019)

21. M.S. Singhvi, S.S. Zinjarde, D.V. Gokhale, Polylactic acid: synthesis and biomedical applications. J. Appl. Microbiol. **127**, 1612–1626 (2019)

22. H. Zhu, J. Ji, R. Lin, C. Gao, L. Feng, J. Shen, Surface engineering of poly(DL-lactic acid) by entrapment of alginate-amino acid derivatives for promotion of chondrogenesis. Biomaterials **23**, 3141–3148 (2002)

23. H. Zhu, A. Ji, J. Shen, Surface engineering of poly (DL-lactic acid) by entrapment of biomacromolecules. Macromol. Rapid Commun. **23**, 819–823 (2002)

24. K.S. Stankevich, N.V. Danilenko, R.M. Gadirov, S.I. Goreninskii, S.I. Tverdokhlebov, V.D. Filimonov, A new approach for the immobilization of poly(acrylic) acid as a chemically reactive cross-linker on the surface of poly(lactic) acid-based biomaterials. Mater. Sci. Eng. C **71**, 862–869 (2017)

25. K.S. Stankevich, A. Gudima, V.D. Filimonov, H. Klüter, E.M. Mamontova, S.I. Tverdokhlebov, J. Kzhyshkowska, Surface modification of biomaterials based on high-molecular polylactic acid and their effect on inflammatory reactions of primary human monocyte-derived macrophages: Perspective for personalized therapy. Mater. Sci. Eng. C **51**, 117–126 (2015)

26. P. Dinarvand, E. Seyedjafari, A. Shafiee, A.B. Jandaghi, A. Doostmohammadi, M.H. Fathi, S. Farhadian, M. Soleimani, New approach to bone tissue engineering: Simultaneous application of hydroxyapatite and bioactive glass coated on a poly(L-lactic acid) scaffold. ACS Appl. Mater. Interfaces **3**, 4518–4524 (2011)

27. E. Baran, H. Erbil, Surface modification of 3D printed PLA objects by fused deposition modeling: A review. Colloids Interfaces **3**, 43 (2019)

28. S. Zeng, J. Ye, Z. Cui, J. Si, Q. Wang, X. Wang, K. Peng, W. Chen, Surface biofunctionalization of three-dimensional porous poly(lactic acid) scaffold using chitosan/OGP coating for bone tissue engineering. Mater. Sci. Eng. C **77**, 92–101 (2017)

29. S. Hassanajili, A. Karami-Pour, A. Oryan, T. Talaei-Khozani, Preparation and characterization of PLA/PCL/HA composite scaffolds using indirect 3D printing for bone tissue engineering. Mater. Sci. Eng. C **104**, 109960 (2019)

30. C.-H. Cheng, Y.-W. Chen, A. Kai-Xing Lee, C.-H. Yao, M.-Y. Shie, Development of mussel-inspired 3D-printed poly (lactic acid) scaffold grafted with bone morphogenetic protein-2 for stimulating osteogenesis. J. Mater. Sci. Mater. Med. **30**, 78 (2019)

31. M. Wang, P. Favi, X. Cheng, N.H. Golshan, K.S. Ziemer, M. Keidar, T.J. Webster, Cold atmospheric plasma (CAP) surface nanomodified 3D printed polylactic acid (PLA) scaffolds for bone regeneration. Acta Biomater. **46**, 256–265 (2016)

32. X. Bai, M. Gao, S. Syed, J. Zhuang, X. Xu, X.-Q. Zhang, Bioactive hydrogels for bone regeneration. Bioactive Mater. **3**, 401–417 (2018)

33. K. Gkioni, S.C.G. Leeuwenburgh, T.E.L. Douglas, A.G. Mikos, J.A. Jansen, Mineralization of hydrogels for bone regeneration. Tissue Eng. Part B Rev. **16**, 577–585 (2010)

34. J. Venkatesan, I. Bhatnagar, P. Manivasagan, K.-H. Kang, S.-K. Kim, Alginate composites for bone tissue engineering: A review. Int. J. Biol. Macromol. **72**, 269–281 (2015)

35. P. Diaz-Rodriguez, P. Garcia-Triñanes, M.M. EchezarretaLópez, A. Santoveña, M. Landin, Mineralized alginate hydrogels using marine carbonates for bone tissue engineering applications. Carbohydr. Polym. **195**, 235–242 (2018)

36. Y.H. Lee, B.W. Lee, Y.C. Jung, B.I. Yoon, H.M. Woo, B.J. Kang, Application of alginate microbeads as a carrier of bone morphogenetic protein-2 for bone regeneration. J. Biomed. Mater. Res. Part B **107**, 286–294 (2019)

37. A. Sosnik, Alginate particles as platform for drug delivery by the oral route: State-of-the-art. ISRNPharm. **2014**, 926157 (2014)

38. M. Rezvanian, M.C.I.M. Amin, S.-F. Ng, Development and physicochemical characterization of alginate composite film loaded with simvastatin as a potential wound dressing. Carbohydr. Polym. **137**, 295–304 (2016)

39. J. Sun, H. Tan, Alginate-based biomaterials for regenerative medicine applications. Materials **6**, 1285–1309 (2013)

40. E.S. Place, L. Rojo, E. Gentleman, J.P. Sardinha, M.M. Stevens, Strontium- and zinc-alginate hydrogels for bone tissue engineering. Tissue Eng. Part A **17**, 2713–2722 (2011)

41. M. Kim, W.-K. Jung, G. Kim, Bio-composites composed of a solid free-form fabricated polycaprolactone and alginate-releasing bone morphogenic protein and bone formation peptide for bone tissue regeneration. Bioprocess Biosyst. Eng. **36**, 1725–1734 (2013)

42. J. Hua, P.F. Ng, B. Fei, High-strength hydrogels: Microstructure design, characterization and applications. J. Polym. Sci. Part B **56**, 1325–1335 (2018)

43. R.A. Pérez, J.-E. Won, J.C. Knowles, H.-W. Kim, Naturally and synthetic smart composite biomaterials for tissue regeneration. Adv. Drug Deliv. Rev. **65**, 471–496 (2013)

44. S. Pina, V.P. Ribeiro, C.F. Marques, F.R. Maia, T.H. Silva, R.L. Reis, J.M. Oliveira, Scaffolding strategies for tissue engineering and regenerative medicine applications. Materials **12**, 1824 (2019)

45. N. Eliaz, N. Metoki, Calcium phosphate bioceramics: A review of their history, structure, properties, coating technologies and biomedical applications. Materials **10**, 334 (2017)

46. J. Kundu, J.-H. Shim, J. Jang, S.-W. Kim, D.-W. Cho, An additive manufacturing-based PCL–alginate–chondrocyte bioprinted scaffold for cartilage tissue engineering. J. Tissue Eng. Regen. Med. **9**, 1286–1297 (2015)

47. R. Donate, M. Monzón, M.E. Alemán-Domínguez, Additive manufacturing of PLA-based scaffolds intended for bone regeneration and strategies to improve their biological properties. e-Polymers **20**, 571–599 (2020)

48. I. Fernández-Cervantes, M.A. Morales, R. Agustín-Serrano, M. Cardenas-García, P.V. Pérez-Luna, B.L. Arroyo-Reyes, A. Maldonado-García, Polylactic acid/sodium alginate/hydroxyapatite composite scaffolds with trabecular tissue morphology designed by a bone remodeling model using 3D printing. J. Mater. Sci. **54**, 9478–9496 (2019)

49. F.A.A. Al-Rub, M.M. Fares, T. Talafha, Poly(acrylic acid) grafted sodium alginate di-block hydrogels as efficient biosorbents: Structure–property relevance. J. Polym. Environ. **26**, 2333–2345 (2018)

50. H. Pirayesh, J.A. Nychka, Sol–gel synthesis of bioactive glass-ceramic 45S5 and its in vitro dissolution and mineralization behavior. J. Am. Ceram. Soc. **96**, 1643–1650 (2013)

51. C.-C. Lin, L.-C. Huang, P. Shen, $Na_2CaSi_2O_6$–P_2O_5 based bioactive glasses. Part 1: Elasticity and structure. J. Non-Cryst. Solids **351**, 3195–3203 (2005)

52. S. Sasaki, T. Asakura, Helix distortion and crystal structure of the α-form of poly(ʟ-lactide). Macromolecules **36**, 8385–8390 (2003)

53. J. Qian, Y. Kang, Z. Wei, W. Zhang, Fabrication and characterization of biomorphic 45S5 bioglass scaffold from sugarcane. Mater. Sci. Eng. C **29**, 1361–1364 (2009)

54. R. Auras, B. Harte, S. Selke, An overview of polylactides as packaging materials. Macromol. Biosci. **4**, 835–864 (2004)

55. S. Shankar, L.F. Wang, J.W. Rhim, Incorporation of zinc oxide nanoparticles improved the mechanical, water vapor barrier, UV-light barrier, and antibacterial properties of PLA-based nanocomposite films. Mater. Sci. Eng. C **93**, 289–298 (2018)

56. J. Dong, Y. Ozaki, K. Nakashima, Infrared, Raman, and near-infrared spectroscopic evidence for the coexistence of various hydrogen-bond forms in poly(acrylic acid). Macromolecules **30**, 1111–1117 (1997)

57. A.C.S. Alcântara, P. Aranda, M. Darder, E. Ruiz-Hitzky, Bionanocomposites based on alginate–zein/layered double hydroxide materials as drug delivery systems. J. Mater. Chem. **20**, 9495–9504 (2010)

58. D.K. Owens, R.C. Wendt, Estimation of the surface free energy of polymers. J. Appl. Polym. Sci. **13**, 1741–1747 (1969)

59. F.E. Ciraldo, E. Boccardi, V. Melli, F. Westhauser, A.R. Boccaccini, Tackling bioactive glass excessive in vitro bioreactivity: Preconditioning approaches for cell culture tests. Acta Biomater. **75**, 3–10 (2018)